BNL-76947-2006-BC

Photoemission as a Probe of the Collective Excitations in Condensed Matter Systems

Peter D. Johnson and Tonica Valla

To be published in "Photoemission"

July 2006

Condensed Matter Physics & Materials Science Department

Brookhaven National Laboratory
P.O. Box 5000
Upton, NY 11973-5000
www.bnl.gov

DISCLAIMER

BNL-76947-2006-BC

Photoemission as a probe of the Collective Excitations in Condensed Matter Systems

Peter D. Johnson and Tonica Valla

Condensed Matter and Materials Science Department, Brookhaven National Laboratory, Upton, NY, 11973

1 Introduction

New developments in instrumentation have recently allowed photoemission measurements to be performed with very high energy and momentum resolution.[1] This has allowed detailed studies of the self-energy corrections to the lifetime and mass renormalization of excitations in the vicinity of the Fermi level. These developments come at an opportune time. Indeed the discovery of high temperature superconductivity in the cuprates and related systems is presenting a range of challenges for condensed matter physics.[2] Does the mechanism of high T_C superconductivity represent new physics? Do we need to go beyond Landau's concept of the Fermi liquid?[3] What, if any, is the evidence for the presence or absence of quasiparticles in the excitation spectra of these complex oxides? The energy resolution of the new instruments is comparable to or better than the energy or temperature scale of superconductivity and the energy of many collective excitations. As such, photoemission has again become recognized as an important probe of condensed matter.

Studies of the high T_C superconductors and related materials are aided by the observation that they are two dimensional. To understand this, we note that the photoemission process results in both an excited photoelectron and a photohole in the final state. Thus the experimentally measured photoemission peak is broadened to a width reflecting contributions from both the finite lifetime of the photohole and the momentum broadening of the outgoing photoelectron. The total width Γ is given by [4]

$$\Gamma = \left(\Gamma_h + \frac{v_h}{v_e}\Gamma_e\right)\left(\left|1 - \frac{v_h}{v_e}\right|\right)^{-1} \quad (1)$$

where Γ_h is the width of the hole state, Γ_e the width of the electron state, and v_h and v_e the respective perpendicular velocities. In a two dimensional system with $v_h = 0$, the width of the photoemission peak is therefore determined entirely by the inverse lifetime or scattering rate of the photohole, Γ_h. This observation offers the possibility that the technique may be useful as a

probe of the related scattering mechanisms contributing to the electrical transport in different materials. Unlike other probes of these transport properties, photoemission has the advantage that it is momentum resolving. In drawing conclusions from such studies, it is important to remember that the single particle scattering rate measured in photoemission is not identical to the scattering rate measured in transport studies, τ_{tr}. However with certain assumptions, the two are approximately related and the transport scattering rate can be written $\hbar/\tau_{tr} = \hbar/\tau\,(1 - \langle\cos\vartheta\rangle)$ where $\hbar/\tau$ represents the single particle scattering rate and $\langle\cos\vartheta\rangle$ represents the average value of $\cos\vartheta$ with ϑ the scattering angle [5, 6].

In the following sections we first review the photoemission process with particular reference to the role of coupling to many body excitations. We then examine in more detail the coupling to a variety of excitations including phonons, charge density waves (CDW) and magnetic or spin excitations. Finally we review studies of the high T_C materials with an emphasis on measurements of self-energy effects. We note that our discussion is heavily concentrated around our own work but recognize the many important studies that have been reported by other groups.

2 The photoemission process

In photoelectron spectroscopy, a photon of known energy, $h\nu$, is absorbed and the outgoing electron's energy ($h\nu - \phi - \varepsilon_k$) and angle are measured. These properties determine the binding energy ε_k and parallel momentum $k_{||}$ of the hole left in the occupied valence bands.[7] Interaction effects, including for instance Coulomb and electron-phonon, cause the sharp line spectrum of independent electron theory, $\mathrm{A_0}(\mathbf{k},\omega) = \mathrm{Im}\ \mathrm{G_0}(\mathbf{k},\omega) = \mathrm{Im}\ 1/(\omega - \epsilon_{\mathbf{k}0} - i\eta)$, where $\epsilon_{\mathbf{k}0}$ represents a bare band dispersion, to evolve into $\mathrm{Im}\ 1/[\omega - \epsilon_{\mathbf{k}0} - \Sigma(\mathbf{k},\omega)]$ where the complex self-energy $\Sigma(\mathbf{k},\omega)$ contains the effects of the many body interactions. The single-particle spectral function of the hole-state, $\mathrm{A}(\mathbf{k},\omega)$, then takes the form

$$\mathrm{A}(\mathbf{k},\omega) \propto \frac{\Sigma_2(\mathbf{k},\omega)}{[\omega - \epsilon_{\mathbf{k}0} - \Sigma_1(\mathbf{k},\omega)]^2 + (\Sigma_2(\mathbf{k},\omega))^2} \tag{2}$$

Thus the real part, $\Sigma_1(\mathbf{k},\omega)$, gives a shift in energy and associated mass enhancement, while the imaginary part $\Sigma_2(\mathbf{k},\omega)$ gives the lifetime broadening $h/\tau_{\mathbf{k}}$. Here $\tau_{\mathbf{k}}$ is the typical time before the hole state $(\omega,\mathbf{k})$ scatters into other states, $(\omega',\mathbf{k}')$. In the limit of $\omega \to 0$, the real part of the self energy may be written as $\Sigma_1(\mathbf{k},\omega) \sim -\omega\lambda_{\mathbf{k}}$ with $\lambda_{\mathbf{k}}$ representing a coupling constant describing the coupling to excitations that scatter the hole from $(\omega,\mathbf{k})$ to other states. The process of coupling is illustrated in figure 1 where we consider coupling to a mode described by an Eliashberg function, $\alpha^2\mathrm{F}$. Here $\alpha^2\mathrm{F}$ represents the product of the density of states of the relevant excitation and a matrix element reflecting the coupling strength.[8] For the present purposes, $\alpha^2\mathrm{F}$ in figure 1(a) is simply

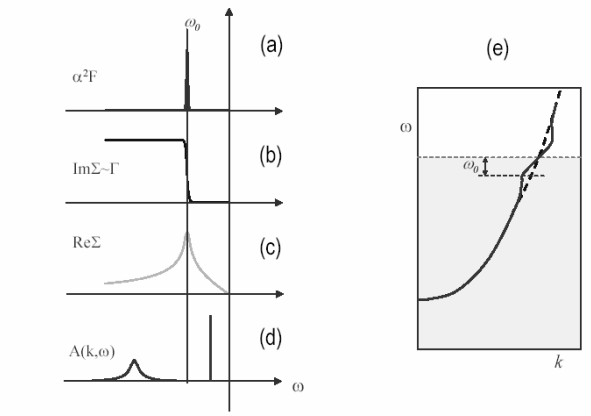

Figure 1: An electron scattering from a mode with $\alpha^2 F$ as in (a) will experience a step function at the mode energy in the imaginary component of its self-energy, ImΣ or Σ_2, as in panel (b). A Kramers-Kronig transform of Σ_2 will produce a cusp function in the real part of the self-energy, ReΣ or Σ_1 as shown in panel (c). The Σ_2 shown in panel (b) results in a spectral function having the form shown in panel (d) above and below the mode energy. Panel 1(e) shows the mass renormalization in the immediate vicinity of E_F.

represented by a single Gaussian peak at energy Ω_0. Coupling to such a mode (at T = 0 K) will result in a broadened step function in the scattering rate or imaginary part of the self energy, Σ_2. The step function reflects the observation that when the photohole has enough energy to create the mode ($\omega \geq \Omega_0$), scattering from the mode opens up a new decay channel, thereby shortening the lifetime. The real and imaginary parts of the self energy are related via causality through a Kramers Kronig transform. Thus the step function in Σ_2 results in a cusp function for Σ_1 (panel (c)). Such an energy dependence of the self energy affects the measured spectra in two ways. Above and below the mode energy there will be a noticeable change in the spectral function as illustrated in panel (d). Secondly, as noted above, the measured dispersion will be given by $\epsilon_{\mathbf{k}0} + \Sigma_1(\mathbf{k},\omega)$. Thus with Σ_1 taking the form shown in panel (c), the dispersion will display the mass enhancement observed immediately below the Fermi level as presented in figure 1(e).

The intensity $I(\mathbf{k},\omega)$ of photoelectrons measured as a result of the photoemission process is given by

$$I(\mathbf{k},\omega) = |M|^2 A(\mathbf{k},\omega) f(\omega) \tag{3}$$

where M represents the matrix element linking the initial and final states in the photoemission process, $A(\mathbf{k},\omega)$ is the single particle spectral function given in equation (2) and $f(\omega)$ is the Fermi function which enters because the photoemission process is restricted to excitation from occupied states. Modern photoelectron spectrometers allow the simultaneous measurement of photoelectron intensities from a finite range in both energy and momentum space. A typical image is shown in figure 2.[9] The ability to obtain such images has led to the development of new methodologies for the extraction of self-energies. As such, the spectral response in figure 2 may be analysed by taking an intensity cut at constant angle or momentum, the so called energy distribution curve (EDC) or by taking an intensity cut at constant energy, a momentum distribution curve (MDC). The former has been the traditional method, the latter is a new method enabled by the new instrumentation. Let us consider the MDC method. If a binding energy is fixed and in the limit of a momentum independent self-energy, the spectral function (MDC) takes the simple form:

$$A(\mathbf{k},\omega_0) = \frac{\Sigma_2(\omega_0)}{[\omega_0 - \epsilon_{\mathbf{k}0} - \Sigma_1(\omega_0)]^2 + [\Sigma_2(\omega_0)]^2} \tag{4}$$

In the vicinity of the Fermi level we may approximate the bare dispersion with a linear form such that $\epsilon_{k0} = v_0(k - k_F)$ with v_0 the bare velocity. As has been discussed in several papers,[10, 11, 12, 13] the MDC is then a simple Lorentzian, centered at $k_m = k_F + [\omega_0 - \Sigma_1(\omega_0)]/v_0$ and with the full width at half maximum $\Delta k = 2\Sigma_2(\omega_0)/v_0$. The self-energy can thus be simply extracted from MDC peaks at any binding energy.

Noting that the measured or renormalized velocity $v = v_0/(1 + \lambda)$, where, as before, λ represents the coupling constant, the equivalent EDC has a width

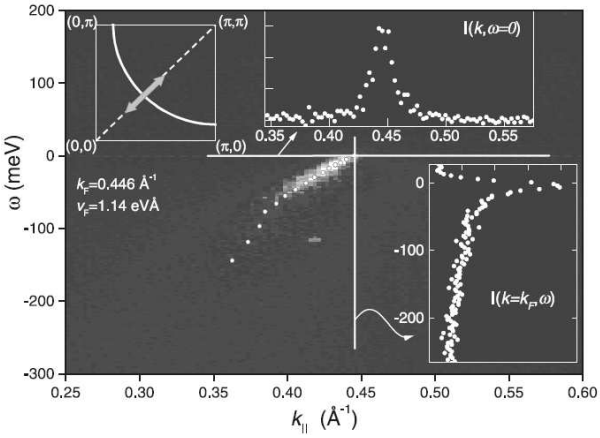

Figure 2: Two-dimensional spectral plot showing the intensity of emission in the (π, π) direction of the Brillouin zone as a function of ω, the binding energy, and $k_{||}$, the parallel momentum. The photon energy is 21.2 eV and the sample temperature is 48 K. Clockwise from upper left, the insets show the region of the Brillouin zone sampled in the experiment, a cross section through the intensity at constant energy ($\omega = 0$) as a function of momentum (an MDC), and a cross section through the intensity at constant angle or momentum ($k = k_F$) as a function of ω (an EDC).

ΔE such that

$$\Delta E = v\Delta k = \frac{2\Sigma_2}{(1+\lambda)} = \frac{2\Sigma_2}{1-\partial\Sigma_1/\partial\omega} \tag{5}$$

If the real part of the self-energy displays no frequency dependence, the width ΔE is directly related to the scattering rate. Both EDCs and MDCs will have a Lorentzian line shape. However this is no longer true if the real part of the self-energy is frequency dependent and particularly in the vicinity of a mode, the width of the EDC, ΔE, will be strongly dependent on the renormalization of the velocity. This can result in the EDC having a complex two peaked structure that is more difficult to interpret.

3 Electron-phonon coupling in metallic systems

In this section we focus on photoemission studies of electron-phonon coupling in metallic systems. The electron-phonon coupling contribution, Γ_{e-ph}, to the total scattering rate may be calculated via the Eliashberg equation such that [5]

$$\Gamma_{e-ph}(\omega, T) = 2\pi\hbar \int_0^\infty d\omega' \alpha^2 F(\omega') \left[2n(\omega') + f(\omega'+\omega) + f(\omega'-\omega)\right] \tag{6}$$

where again $\alpha^2 F$ is the Eliashberg coupling constant and $f(\omega)$ and $n(\omega)$ are the Fermi and Bose-Einstein functions, respectively. Γ_{e-ph} increases monotonically with energy up to some cut-off defined by the Debye energy. At $T = 0$ K the electron-phonon coupling constant is given by [8]

$$\lambda = 2\int_0^\infty \frac{\alpha^2 F(\omega')}{\omega'} d\omega' \tag{7}$$

Early photoemission studies focused on the observation that at higher temperatures, above approximately one third the Debye energy, equation (6) reduces to $\Gamma_{e-ph} = \pi\lambda k_B T$. Thus a measurement of the width of a photoemission peak as a function of temperature provides direct access to the coupling constant, λ. This approach has been used in several studies including a study of the electron-phonon contribution to quasiparticle lifetimes of surface states on the Cu(111) [14] and Be(0001) [15] surfaces. In the former case the electron-phonon coupling constant for the surface, $\lambda = 0.14$ was close to that measured for bulk copper, $\lambda = 0.15$. In the case of Be, the surface was found to have a dramatically enhanced value of $\lambda = 1.15$, which is to be compared with the bulk value of $\lambda = 0.24$. Hengsberger *et al.* found a similar value, $\lambda = 1.18$, for the electron-phonon coupling parameter in the surface region of Be by measuring the velocity renormalization in the surface band.[16] However the most recent study of the same surface reduced the value λ to 0.7, a value obtained from a determination of the rate of change of the real part of the self-energy,$-(\partial\Sigma_1/\partial\omega)$, in the vicinity of

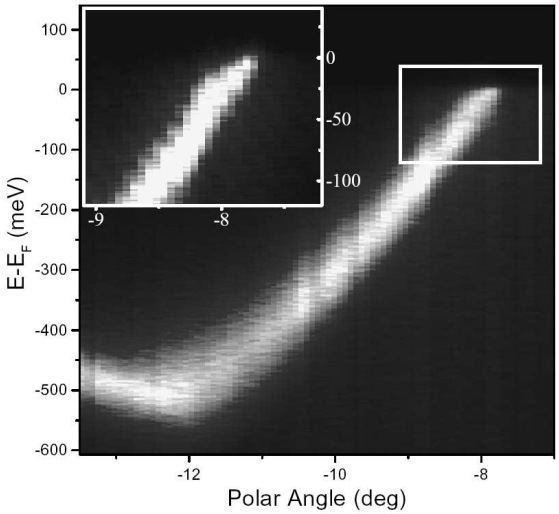

Figure 3: ARPES intensity plot of the Mo(110) surface recorded along the $\Gamma - N$ line of the surface Brillouin zone at 70 K. Shown in the inset is the spectrum of the region around k_F taken with special attention to the surface cleanliness.

E_F. Enhanced values of λ have led to speculation on the possibility of enhanced superconducting transition temperatures in the surface region.[15]

The introduction of the new instrumentation in the nineties allowed the first direct imaging of the mass renormalization due to electron-phonon coupling. Fig. 3 shows an image of the spectral intensity excited from a two-dimensional surface resonance in the Γ -N azimuth of a Mo(110) crystal with the sample held at 70 K.[17] The state shown in the figure corresponds to a surface resonance which closes an elliptical hole Fermi orbit around the center of the zone, $\overline{\Gamma}$.[18] In the vicinity of the Fermi level there is a notable change in the rate of dispersion, or mass enhancement, and a rapid change in the width of the band. The self energy corrections resulting in these changes reflect three principal contributions, electron-electron scattering, electron-phonon scattering and electron-impurity scattering. These different contributions all add linearly to give the total scattering rate Γ such that

$$\Gamma = \Gamma_{e-e} + \Gamma_{e-ph} + \Gamma_{imp} \tag{8}$$

In a Fermi liquid the electron-electron scattering term is given by $\Gamma_{e-e}(\omega, T) = 2\beta\left[(\pi k_B T)^2 + \omega^2\right]$ where, within the Born approximation, $2\beta = (\pi \mathrm{U}^2)/(2\mathrm{W}^3)$, with U the on-site Coulomb repulsion and W the bandwidth of the state. As noted earlier the electron-phonon contribution may be calculated via the Eliashberg equation, eq. (6). The final contribution in equation (8), impurity scattering, is elastic in that the impurity atoms are considered to have no internal excitations. Thus the scattering-rate, Γ_{imp}, is proportional to the impurity

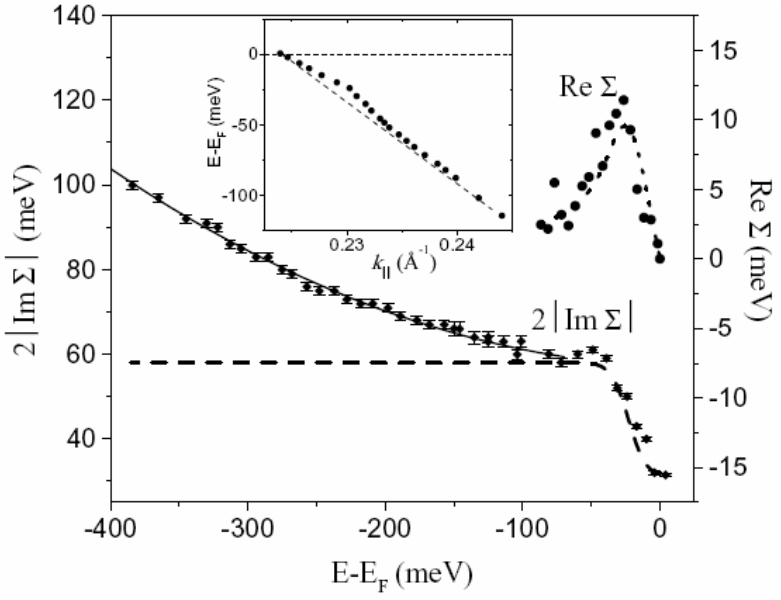

Figure 4: The photohole self-energy as a function of binding energy at 70 K. The real part is obtained from the MDC-derived dispersion shown in the inset. The imaginary part is obtained from the width of the quasiparticle peak. The solid line is a quadratic fit to the high-binding energy data ($\omega < 80$ meV). The dashed (dotted) line shows the calculated electron-phonon contribution to the imaginary (real) part of the self-energy. The dashed line is shifted up by 26 meV.

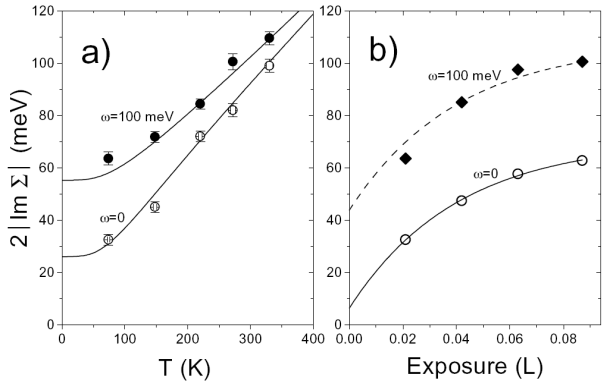

Figure 5: The peak width as a function of (a) temperature and (b) exposure to background hydrogen, measured for two binding energies. For the exposure dependence the sample was held at 70 K. Lines in (a) are calculated electron-phonon contributions, shifted up by 26 meV to match the data. Lines in (b) represent fits (see text for details).

concentration, but independent of energy and temperature. At sufficiently low temperature, impurity scattering represents the dominant decay mechanism for a hole close to E_F.

Figure 4 shows the measured Σ_2 of the Mo surface state as a function of binding energy. The data points are extracted from the image of fig. 3 in two ways, either from EDCs or from MDCs. The calculated electron-phonon contribution to the self-energy is indicated in the figure. In the vicinity of the Fermi level, the agreement between the calculation using the theoretical α^2F of bulk molybdenum.[19] and the experimentally measured widths is excellent. There is a rapid change in the scattering rate up to the Debye energy at ~ 30 meV. At binding energies greater than this, the electron-phonon contribution saturates. However, also shown in the figure is a quadratic fit to the measured widths at the higher binding energies. The quadratic dependence is an indication that electron-electron scattering, as in a Fermi liquid, plays an important role. In a purely two dimensional system there should be a logarithmic correction to the quadratic term.[20] Thus Γ_{e-e} will be proportional to $\omega^2 \ln\omega$. However the simple quadratic fit works well as indicated in the figure because the surface state shown in figure 3 is, as previously noted, a surface resonance with good coupling to bulk states.[18] The quadratic fit is consistent with the prefactor in the expression for Γ_{e-e} having U$\sim$0.6 eV, as predicted for molybdenum,[21] and W$\sim$1.3 eV the approximate bandwidth of the surface state. The measured widths also have an energy-independent contribution due to scattering from hydrogen impurity centers.[17]

The calculated real component of the self energy, Σ_1, derived through a Kramers Kronig transform of Σ_2 is also shown in figure 4 where it is compared

with the experimentally derived values. From Σ_1 it is possible to determine a value for the electron-phonon coupling constant of 0.4 to be compared with the bulk value of 0.42. As we have already noted the coupling constant can also be derived from the temperature dependence of the peak widths. This is shown in figure 5(a) for two different binding energies, $\omega = 0$ and $\omega = 100$ meV. By doing linear fits to the experimental data points, values for the coupling constant of 0.52 and 0.35 are obtained respectively. These values are again close to the bulk value.

The observation that the width of the quasiparticle peak always has a significant constant term indicates the presence of impurity scattering. It is known that this surface state is very sensitive to hydrogen adsorption. Fig. 5(b) shows how the width changes with the exposure to residual hydrogen. Note that it saturates with exposure θ. If the scattering rate is proportional to the concentration of adsorbed particles, the experimental points become a measure of the concentration. Since the number of free adsorption sites decays exponentially with exposure, the concentration of adsorbed atoms as a function of exposure should change as $c(\theta) = c_0 + c_{sat}(1 - e^{-p\theta})$, where p is the adsorption probability and c_0 (c_{sat}) is the initial (saturation) concentration. The width of the quasiparticle peak can be fitted with the same dependence (lines). It is notable that extrapolation to zero exposure results in a residual width of 6 ± 5 meV at $\omega = 0$. Electron-phonon coupling contributes with ≈ 5 meV for T=70 K. However, we should also note that there is some uncertainty in the initial coverage due to the change in adsorption conditions between flashing the sample and the measurement.

4 Studies of the dichalgogenides

The family of layered dichalcogenides provide a range of interesting phenomena for study. These systems exhibit both charge-density wave (CDW) formation and superconductivity.[22, 23] As shown in figure 6, the fact that the CDW transition temperature decreases while the superconducting critical temperature, T_C, increases on going from $TaSe_2$ through TaS_2 and $NbSe_2$ to NbS_2 suggests that the two order parameters represent competing ground states. Indeed, it has been found that in TaS_2 and $NbSe_2$, T_C increases under pressure while T_{CDW} decreases [24, 25] While these studies suggested that after CDW order disappears, T_C remains approximately constant, a more recent study of $NbSe_2$ indicates that as a function of pressure, T_C at first increases up to some maximum vale and then decreases.[26] In NbS_2, the system with no CDW order, T_C is insensitive to pressure. Although various anomalies, including an apparent anisotropy of the superconducting gap, have been observed, [27, 28, 29, 30] it is generally believed that superconductivity in the dichalcogenides is of the conventional BCS character, mediated by strong electron-phonon coupling [29]. However, consensus on the exact mechanism that drives the system into the CDW state has still not been reached. Some authors [22, 23, 31, 32] argue, in analogy with a Pierels transition in one- dimensional systems, that the CDW

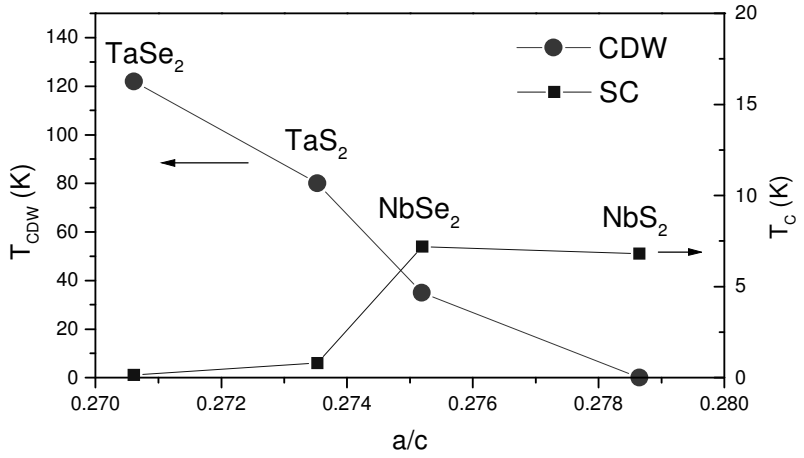

Figure 6: A comparison of the CDW transition temperature T_{CDW} and the superconducting transition temperature T_C for the dichalcogenides plotted as a function of the ratio of lattice parameters a/c.(Reproduced from Ref. [23])

transition is driven by a Fermi surface instability or nesting, with some portions of the Fermi surface spanned by a CDW vector- q_{CDW}. In another scenario, the CDW instability is induced by the nesting of van Hove singularities or saddle points in the band structure if they are within a few $k_B T_{CDW}$ of the Fermi energy.[33]

The Fermi surface of the 2H dichalcogenides is rather complicated, being dominated by several open (2D-like) sheets and one small 3D S(Se)-derived pancake-like Fermi surface.[29] In such a situation, one may anticipate anisotropic properties and in particular, an anisotropic electron-phonon coupling. The resistivity anisotropy, of the order of 10-50, is much smaller than in layered oxides, indicating a substantial inter-layer hopping.[34] Transport properties show relatively small anomalies at T_{CDW}, suggesting that only a small portion of the Fermi surface becomes gapped in the CDW state. In addition, the 2H dichalcogenides become better conducting in the CDW state, indicating a higher degree of coherence.

Several ARPES studies of the dichalcogenides have measured the form or shape of the Fermi surface, the focus being on the identification of the appropriate nesting vector associated with the CDW. In figure 7 we reproduce the results of a recent study showing the measured Fermi surfaces of both $TaSe_2$ and $NbSe_2$.[35] The figure also shows superimposed the results of a simple tight binding fit by the authors of the study to the electronic structure.

Our own study of $TaSe_2$ [12] found, as in earlier studies, [36, 37, 38]that the hole pocket at the center of the zone remains ungapped even in the CDW state. However the studies of the electronic states forming this Fermi surface found strong evidence of the formation of the CDW state as shown in figure 8. The

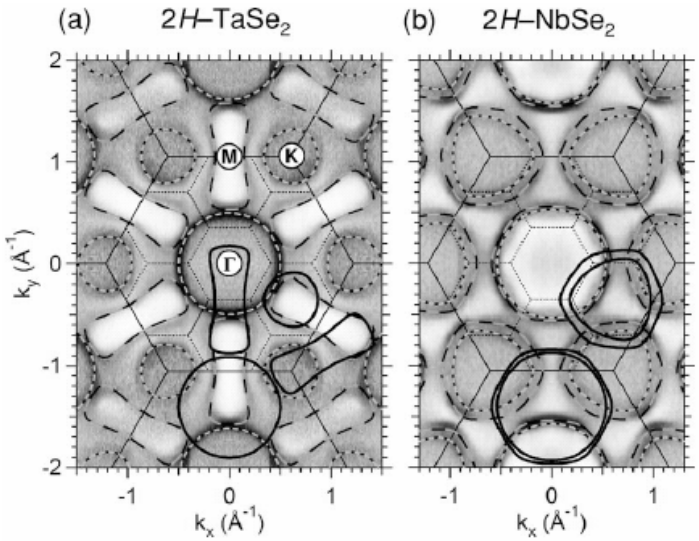

Figure 7: E_F-ARPES intensity maps of (a) 2H-TaSe2 and (b) 2H-$NbSe_2$, measured in the normal states at 125 and 65 K, respectively ($h\nu$ =100 eV). Raw data are shown in the upper right quadrants. The rest of the data is obtained by mirror symmetry operations. The intensity value at each k point is normalized by the intensity integrated over the occupied transition-metal d bandwidth ($\sim$400 meV). The darker grayscale indicates higher photoemission intensity. The small-dotted hexagons are the Brillouin-zone scheme for the 3×3 superlattice. Short and long dashed lines: Simulated Fermi contours of two transition-metal d-derived bands. Solid lines in the lower right quadrants: Umklapp shifted Fermi contours. (reproduced from Ref. [35])

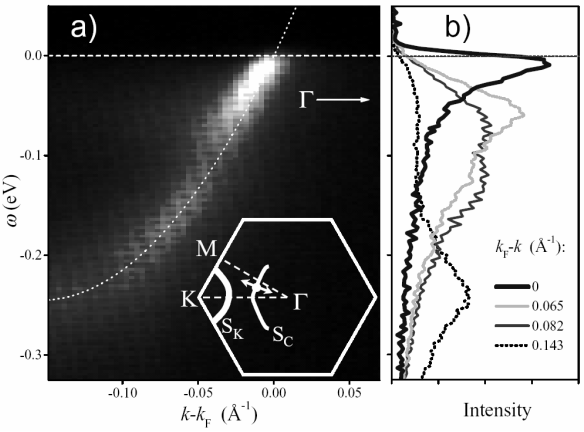

Figure 8: The photoemission intensity in the CDW state (T = 34 K) as a function of binding energy and momentum along the line indicated in the inset by the double-headed arrow. The intensity is represented by a false color map, with yellow and white representing the highest intensity. The dispersing state is a part of the hole like Fermi surface S_C, centered at Γ. This Fermi surface is not gapped in the CDW state. (b) EDCs, measured for several momenta as discussed in the text.

figure shows the photoemission intensity, recorded in the CDW state at $T = 34$ K, as a function of binding energy and momentum along the line through the two-dimensional Brillouin zone indicated in the inset of the figure. A band is observed crossing the Fermi level at a point on the hole-like Fermi surface S_C, centered at Γ. The Fermi surface of dichalgogenides is double walled, suggesting that every band should be split into two.[36, 37] Indeed, in our own study [12] we detected both bands and observed that the splitting, as well as the relative intensity of the two bands, is strongly dependent on momentum, photon energy, polarization and surface quality. In some circumstances, only one band can be observed. However, when both bands are well resolved, they show similar behavior in the vicinity of the Fermi level and similar self-energy corrections. Therefore the presence (or absence) of the second band would appear irrelevant. The most remarkable feature in figure 8 is the "kink" in the band's dispersion, accompanied by a sharpening in the vicinity of the Fermi level. The figure also shows EDC cuts through the intensity at constant momenta. In this energy range, the EDCs show a two-peaked structure, behavior that is again characteristic of the interaction of the photohole with some excitation of the system with energy range limited approximately to the energy scale of the kink. As discussed earlier and presented in equation (4), the real and imaginary components of the self-energy, $\Sigma_1(\omega)$ and $\Sigma_2(\omega)$, can be extracted directly from a momentum-distribution curve. The fitting is possible without imposing any particular model for the interaction. The non- interacting dispersion in figure 8

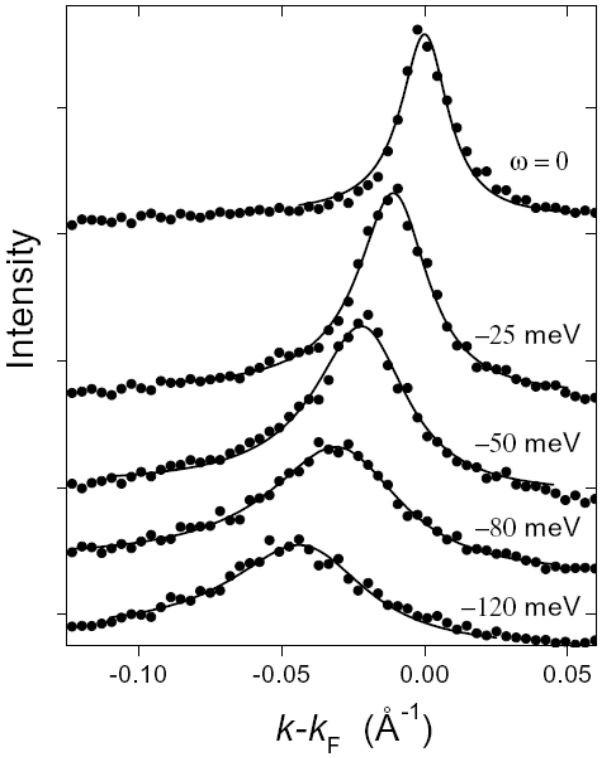

Figure 9: MDCs, measured at different binding energies (symbols), fitted with a momentum-independent spectral function (solid lines) as discussed in the text.

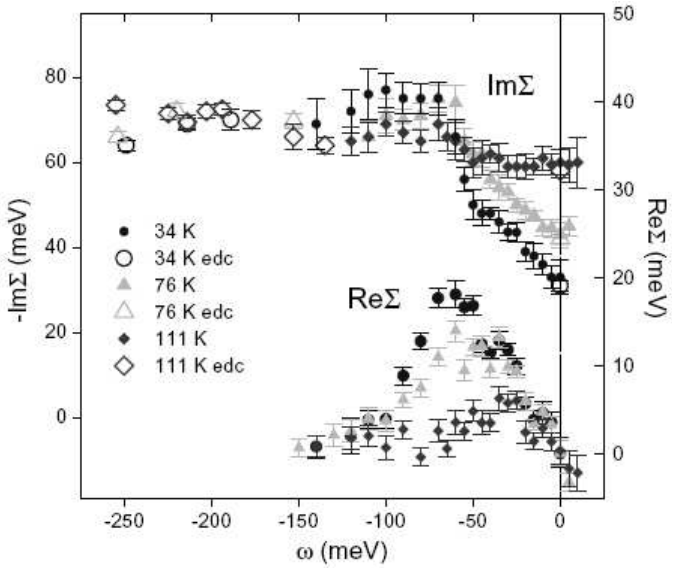

Figure 10: Self-energies extracted from MDCs for several temperatures (solid symbols). Results for Σ_2 obtained from EDCs are shown as open symbols.

may be approximated with a second-order polynomial that coincides with the measured dispersion at $k = k_F$ and at higher binding energies, close to the bottom of the band: thus $\Sigma_1 = 0$ for $\omega = 0$ and for $\omega < -200$ meV. Figure 9 shows several MDCs with corresponding fits. In contrast to the lineshapes in figure 8(b) for EDCs, the lineshapes in figure 9 are approximately Lorentzian at low binding energies developing an asymmetry at higher binding energies. The latter asymmetry mostly reflects the quadratic term in the non-interacting dispersion. The advantage of using MDCs in the analysis is obvious in that the self-energies are more dependent on energy than on momentum.

The results of the fitting procedure, which produces pairs of Σ_1 and Σ_2 for every MDC are shown in Fig. 10 for several temperatures. Σ_2 as obtained by fitting EDCs when the latter have a Lorentzian lineshape are also included. The real part of the self-energy is concentrated in the region of binding energies less than 150 meV. At the lowest temperature, it has a maximum at a binding energy of $\sim$ 65 meV, approximately coincident with the value corresponding to the sharp drop in Σ_2. Such behavior is indicative of the scattering of the photo-hole from some collective excitation or "mode" of the system. The striking similarity with the behavior observed in ARPES studies of a photo- hole interacting with phonons [16, 17] would point to the electron-phonon coupling as the source of this behavior. However this would imply the presence of $\sim$ 70 meV phonons in the CDW state where the highest calculated and measured phonon frequency is $\sim$ 40 meV.[39] The measured temperature dependence of the self-energy also

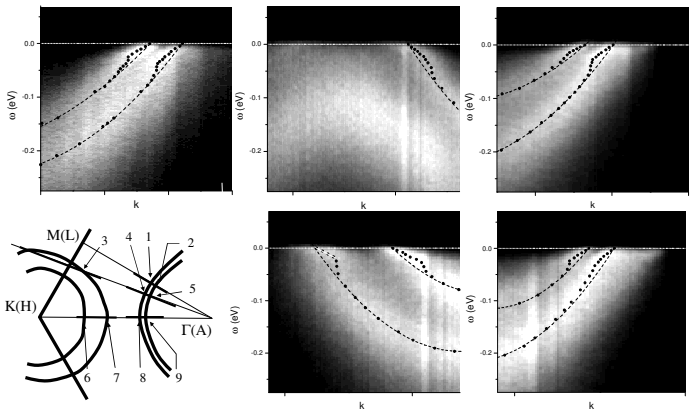

Figure 11: The photoemission intensities in the CDW state at T= 10 K for several momentum lines indicated in the schematic view of the Brillouin zone (lower left panel) by the dark-gray lines. The light-gray lines represent Nb-derived Fermi sheets. The nine Fermi points are numbered. The MDC derived dispersions are represented by full circles. The high-energy part of the dispersions is fitted with a second-order polynomial (dashed lines), and the low energy part is fitted with straight lines.

argues against phonons. With increasing temperature, the peak in Σ_1 loses its magnitude and the structure shifts to lower energies. At a temperature of 111 K, only a small peak is left at a binding energy of $\sim$ 30 meV and this survives in the normal state to at least 160 K. The latter peak may be of the same CDW origin, but may also be caused by conventional electron-phonon coupling, since it is within the range of the phonon spectrum. At low temperatures the imaginary part of the self-energy or scattering rate shows a sharp reduction for binding energies lower than 70 meV. As the temperature increases, this reduction becomes less pronounced.

In a more recent photoemission study,[35] it has been suggested that the higher energy "kink" observed in $TaSe_2$ is associated with a band folding associated with the CDW transition. However it is important to note that the study of Rossnagel *et al.*[35] was at a lower energy resolution and the authors reported a lack of observation of causality, i.e. no defined relationship between the measured real and imaginary parts of the self energy. This differs from the results of the studies discussed here and shown in figure 10. We believe that the high-energy kink is closely related to the CDW gap, either in a conventional way, where the kink will shift from phonon frequency Ω to $\Omega+\Delta_q$ where Δ_q represents the (CDW) gap that opens in the final state at scattering vector q, or in a more exotic way, where a new excitation, or a fluctuation of magnitude of the CDW order parameter, couples to holes and produces the mass enhancement.

Studies of the related system $NbSe_2$ show somewhat different behavior.[40]

Figure 11 shows the photoemission intensity, recorded at T =10 K, as a function of binding energy and momentum along three different momentum lines in the Brillouin zone. Nine Fermi crossings are included: three pairs on the double-layer split Fermi sheets centered around Γ and three crossings on the split sheets centered at the K point. A characteristic change in the quasiparticle velocity ("kink") can easily be identified in all crossings. The kinks are also accompanied by a sharp change in the quasiparticle widths at the "kink" energy. These observations are again indicative of (bosonic) excitations interacting with the quasiparticles. Compared to $TaSe_2$, the excitation spectrum in the CDW state is limited to significantly lower energies. It also appears that the kink is not unique; its strength and energy depend on k, being different for different crossings. The band dispersions in the figure are determined from the peak intensities of MDCs fitted to the spectra. As shown in the figure, the high-energy part of the extracted dispersion can be fitted with a parabola that crosses through k_F , whereas the low energy part ($\omega < 15 - 20$ meV) is fitted with a straight line. Assuming that the parabola represents the "non-interacting" dispersion, then the slopes of these two lines at $\omega = 0$ may be used to directly extract the coupling constant, again using the expression $\lambda = v_0/v_F - 1$ with v_0 the "non-interacting" or bare Fermi velocity and v_F the renormalized one. The "non-interacting" parabolas are subtracted from the measured dispersions to extract $\Sigma_1(\omega)$. The results are shown in Fig. 12(a) for several crossings from Fig. 11. $\Sigma_1(\omega)$ gives the same coupling constant $\lambda = -(\partial\Sigma_1/\partial\omega)_0$, but also provides additional information about the spectrum of excitations interacting with the quasiparticles. It is obvious from Fig. 12(a) that not only is the magnitude of $\Sigma_1(\omega)$ different for different states, but also the peaks are at different energies, ranging from ~ 13 meV to ~ 35 meV. Various experimental and theoretical studies have shown that the phonon spectrum is fully consistent with these energies, with acoustical phonon branches lying below $\omega \sim 12$ meV, and optical branches spanning the region $15 < \omega < 40$ meV.[41] Shifts of the $\Sigma_1(\omega)$ maxima would further suggest that some electronic states are coupled predominantly to acoustic modes while others couple more strongly to the optical modes, even though the states are sometimes very close in momentum (compare points 4 and 5, for example). A strong k-dependence of Σ would complicate the MDC line-shape in the energy region where the momentum dependence exists. It is interesting that in spite of these differences in Σ, the resulting coupling constant does not vary much, $\lambda \sim 0.85 \pm 0.15$, within the experimental uncertainty. The only exception is the inner K-centered sheet (point 6 in figure 11), where $\lambda \sim 1.9 \pm 0.2$. This seemingly too large coupling constant is however in good agreement with the large measured value of linear specific heat coefficient, $\gamma \sim 18.5$ mJmol^{-1}K^{-2}, [27, 42] which is proportional to the renormalized density of states (DOS) at the Fermi level, N(0)(1+λ), through $\gamma = (1/3)\,\pi^2 k_B^2 N\,(0)\,(1+\lambda)$. Band structure calculations give the "bare" DOS N(0) ~ 2.8 states eV^{-1} unit cell^{-1},[29] suggesting $\lambda \sim 1.8$. However even this might be an underestimate as γ measures an average over the Fermi surface, weighted by the DOS. A similar value for λ is obtained from c-axis optical conductivity [43] suggesting that the c-axis transport is probably dominated by the

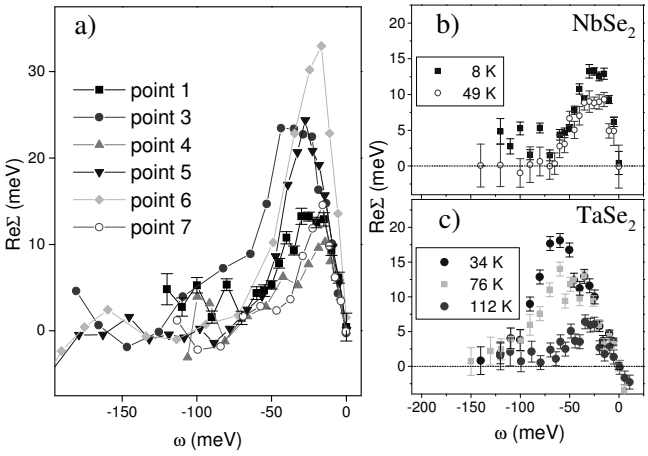

Figure 12: (a) Real parts of self-energies, ReΣ, extracted from measured dispersions from Fig. 11 for several Fermi points. Temperature dependence of $\Sigma_1(\omega)$ for (b) $NbSe_2$ for point 1 from Fig. 11 and for (c) $TaSe_2$ near the same region on the Γ-centered Fermi surface reproduced from figure 10 for comparison.

K-H centered cylinders with largest warping.

It is instructive that in $TaSe_2$ the CDW gap opens up in the same region of the Fermi surface,[35, 37, 44] while the Γ-A centered Fermi cylinders remain ungapped, and gain coherence in the CDW state.[12] It therefore seems plausible that both the superconductivity and the CDW state originate from the inner K sheet and are driven by strong electron-phonon coupling. This seems to be in line with the original suggestion of Wilson [31] that the self-nesting of the inner K sheet drives the CDW in the 2H-dichalcogenides. A lack of CDW gap on the Γ centered sheets in all the 2H-dichalcogenides studied in ARPES suggests that these sheets support neither the self-nesting nor the nesting which would mix them with the K-centered sheets. In particular, a proposed f-wave symmetry for the CDW gap [23] may be ruled out. The relative strength of the CDW and superconducting ordering is determined by the nesting properties of the inner K cylinder, while the upper limit for T_C (when the CDW is destroyed by applying pressure, for example) is given by λ. Nesting weakens with increasing 3D character (increased warping with k_Z) under pressure and on moving from $TaSe_2$ to NbS_2. The coupling constant, λ increases from $TaSe_2$ to $NbSe_2$ and is only weakly pressure dependent. ARPES studies of $NbSe_2$,[30] [45] [46] have shown no evidence of a CDW gap suggesting that the nested portion of the Fermi surface is small and not sampled. However as there is a non-trivial k_Z-dispersion or warping in this material, it is possible that the in-plane k_F might be tuned into a nesting configuration and that the gap opens only near certain k_Z. Note that the energy splitting between the double walled sheets is larger for K-centered sheets. A similar k-dependence is also expected for the interlayer

hopping, $t_\perp$, that produces the warping. Additionally, as the Fermi velocities are larger for Γ- centered sheets, it is reasonable to expect that the in-plane k_F varies with k_Z much less on the Γ-cylinders than on the K-cylinders (the change in the in-plane Fermi momentum is approximately given by $\Delta k_F \propto t_\perp / v_F$). The measured Fermi surfaces centered at Γ are too large at the sampled k_Z, and are therefore not expected to ever reach the self-nesting condition $2k_F = q_{CDW}$. On the other hand, the inner K-centered sheet seems to be very close to producing the required nesting. It is interesting to note that according to STM studies,[47] the CDW gap is large ($\Delta_{CDW} \sim 35$ meV) and should be easily measurable in ARPES. The overall electronic properties in $NbSe_2$ are much less sensitive to the CDW transition than in $TaSe_2$. Even the CDW induced structure in the self-energy that existed in $TaSe_2$ is absent in $NbSe_2$. Both the "kink" and the scattering rate are remarkably insensitive to the CDW (See Fig. 12 b), an observation that is consistent with the relative positions of $NbSe_2$ and $TaSe_2$ in figure 6.

5 Magnetic systems

In magnetic systems, aside from phonon scattering, the possibility also exists for scattering from spin excitations. Such effects have been found in photoemission studies of gadolinium[48] [49] and of iron.[50] The spin dependent electronic structure of these materials has been studied with spin-resolved photoemission.[51] However there has only been one such study with sufficiently high energy resolution to examine in detail the spin resolved self-energy effects. That is a study of gadolinium.[49]

The ground state of gadolinium is ferromagnetic with a Curie temperature T_C of 293 K. The (0001) surface of this material has been shown both theoretically [52] and experimentally [53] to support a surface state derived from the Gd $5d$ orbitals. The state, which is spin polarized through an exchange interaction with the localized $4f$ orbitals has an important history and indeed it was spin-resolved photoemission studies of the surface state that finally confirmed that the surface moments were ferromagnetically aligned with the bulk of the material.[54]

Figure 13 shows spectral density maps recorded from the clean Gd(0001) surface in the ΓX azimuth at two different temperatures.[48] The EDC width of the surface state at a binding energy of ~ 170 meV increases as the temperature is raised from 82 K to 300 K. The increase reflects a reduction in the lifetime of the photohole as a result of increased electron-phonon and electron-magnon scattering at the higher temperature. In the low temperature plot, the state has a width approximately constant until the angle of emission exceeds 5°. At this point, according to calculated band structures,[52] the surface state leaves the bulk band gap and begins to resonate with bulk bands. This accounts for the increased broadening or reduced lifetime. Figure 14 shows the width of the peak as a function of temperature and also shows a fitting to the data points using the expression given in equation (6). The latter results in a value of $\lambda \sim 1.0$ for the

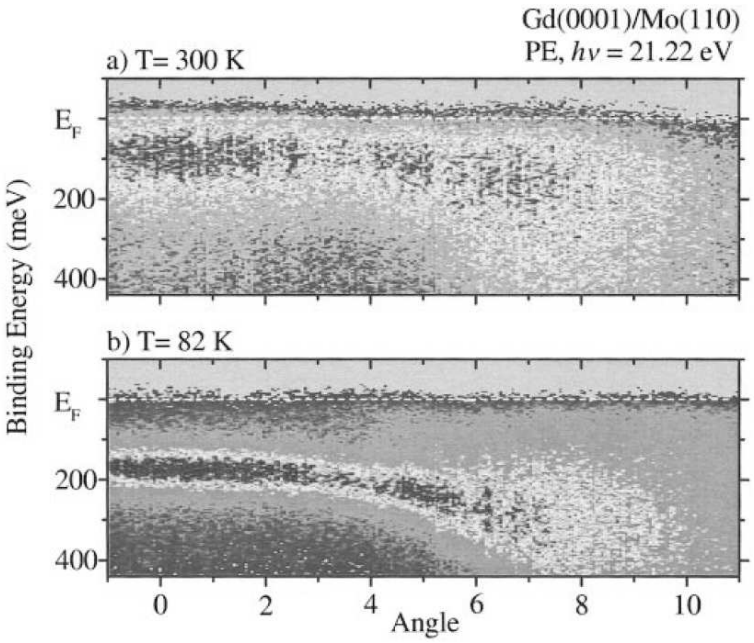

Figure 13: Upper panel: Spin-integrated spectral response for the Gd(0001) surface as a function of binding energy and angle of emission measured from the surface normal. The sample T is 300 K and the incident photon energy is 21.2 eV. Lower panel: As above but now the sample T is 82 K.

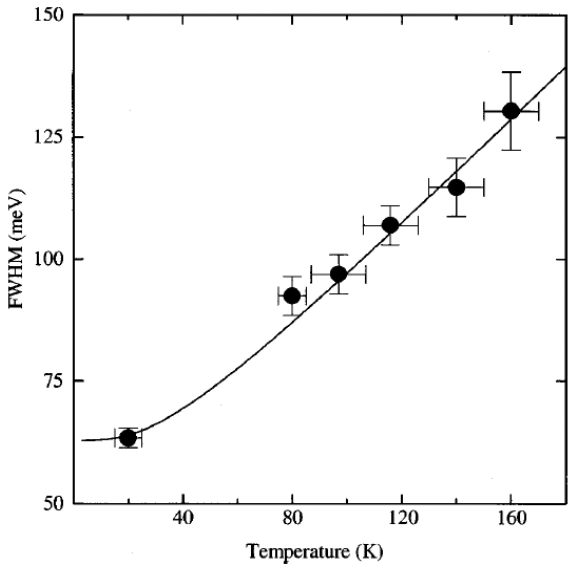

Figure 14: The full width-half maximum (FWHM) of the majority spin peak as a function of T. The solid line indicates a fit to the data using Eq. (6) as given in the text.

electron-phonon coupling constant, which may be compared with a value of 1.2 (bulk, spin averaged), extracted from the measured specific heat,[55] using the calculated density of states and assuming only electron-phonon renormalization, and a theoretical value of 0.4 (also bulk and spin-averaged) obtained in a spin-polarized calculation of the electron-phonon coupling constant.[56] At the low temperatures indicated in figure 13 the state is predominantly majority spin. The electron-phonon coupling parameter may be written as $\lambda = N_S\langle I_S^2\rangle/M\langle\omega^2\rangle$ where N_S represents the spin-projected density of states at the hole binding energy, $\langle I_S^2\rangle$ is the Fermi surface average of the electron-phonon matrix element, M is the atomic mass and $\langle\omega^2\rangle$ is an average phonon frequency. Wu *et al.* have calculated an enhanced magnetic moment in the Gd surface layer.[52] Using their calculated majority and minority spin densities in the surface layer, one obtains $\lambda \sim 1.15$ and 0.25 for the surface majority and minority spin electron-phonon coupling, close to the value $\lambda = 1$ derived from the plot of figure 14 and again assuming that the latter is dominated by the majority spin channel.

The results of a spin resolved photoemission study of the same surface state held at T = 20 K are illustrated in Fig. 15.[49] As noted earlier, both experiment[54, 57] and theoretical calculations [52] indicate that the surface state should be 100% majority spin, reflecting parallel alignment of the surface and bulk moments. The coexistence of both spin components at the same energy in figure 15 is therefore an intrinsic property of the surface state arising from a combination of spin-orbit and spin exchange processes. A simple model yields

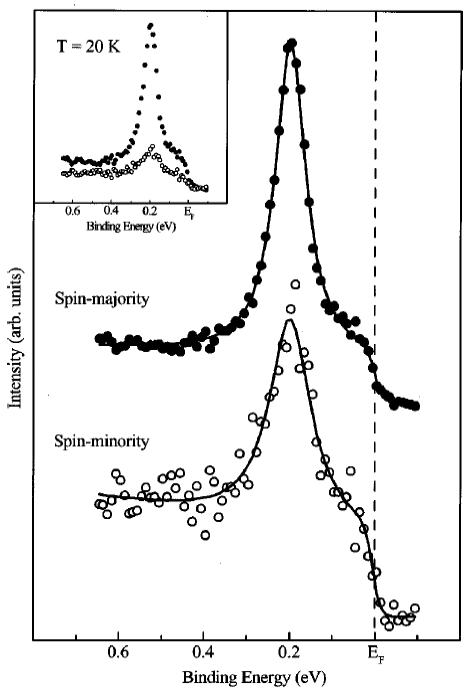

Figure 15: Spin-resolved photoemission spectra recorded from the Gd(0001) surface at 20 K. The upper and lower spectra represent the emission in the majority- and minority-spin channels, respectively. The lines indicate Lorentzian fits to the spectra superimposed on appropriate backgrounds. The inset shows the relative intensities in the two spin channels.

a polarization $P = \Delta/\sqrt{\Delta^2 + \xi^2}$ for each quasiparticle state. With a spin-orbit parameter $\xi = 0.3$ eV and an exchange splitting $\Delta = 0.7$ eV at 0 K, we get a spin-orbit induced mixing $R = (n^+/n^-) = (1\text{-P})/(1\text{+P}) \sim 5\%$. Here n^+ and n^- represent the number of electrons with spin-up and spin-down, respectively. R increases to 8% at T=150 K as the exchange splitting between the occupied and unoccupied surface states gets smaller.[58]

Fitting the spectra in figure 15 with Lorentzian line shapes shows that the minority spin peak has a larger width than its majority spin counterpart, 116 meV as opposed to 86 meV. Removing the contribution from the experimental resolution, these widths become approximately 105 meV in the minority spin channel and 70 meV in the majority channel. Electron-phonon, electron-magnon and electron-electron scattering each give distinct spin dependent contributions to the scattering rate. Electron-electron scattering by exchange processes favors the two holes in the final state being of opposite spin.[59] From consideration of the total density of states in the spin channels, we estimate the scattering rate from this process to be equal for a majority spin hole and a minority spin

hole. The electron-phonon and impurity scattering rate are proportional to the density of states at the hole binding energy for the same spin while the electron-magnon rate is proportional to the density of states for the opposite spin. Since the majority-spin density of states is large while the minority-spin part is small, impurity and electron-phonon scattering should be more important in the majority spin channel. The observation that the minority spin channel is broader suggests electron-magnon scattering is the dominant decay mechanism. At T=0 K, the minority-spin component of a photo-hole can scatter to the majority spin component of a hole state higher in the surface band by emitting a spin wave (tilting the spins of the localized f-electrons). The corresponding spin-flip process is not available to the majority-spin component of the photo-hole at T=0 because the localized f-spins have saturated magnetization and are not able to tilt upwards when the hole tilts down. At higher temperatures, inelastic scattering can occur back and forth between the two spin channels mediated by the emission or absorption of magnons, but the minority-spin component always has the higher density of final states to scatter into. An approximate treatment[60] using the "$s-f$ " Hamiltonian[61] found the result

$$\hbar/\tau(\downarrow) = \frac{\sqrt{3}}{4}\frac{P'(\uparrow)m^*}{S}\left(\frac{2JSa}{\hbar}\right)^2 \tag{9}$$

for the decay of the minority ($\downarrow$) spin component due to spin flip scattering with magnon emission. Here J is the $s-f$ exchange parameter giving the exchange splitting $2JS = 0.65$ eV measured for the surface state,[58] $m^* = 1.21m_e$ is the effective mass measured for the surface band, and $P'(\uparrow)$= 0.87 is the experimentally measured majority component of the band. With S = 7/2 and $a = 3.6$ Å, $\hbar/\tau(\downarrow) \approx 0.095$ eV. Conversely, replacement of $P'(\uparrow)$ by $P'(\downarrow) = 1 - P'(\uparrow)$ gives $\hbar/\tau(\downarrow) \approx 0.014$ eV for the majority spin component. Thus at low T, the majority spin channel is dominated by electron-phonon scattering whereas the minority spin channel is dominated by electron-magnon scattering. Based on the relative spin-dependent densities of states it is possible to provide estimates of the contribution of phonon scattering in the two spin channels. These would be 46 meV in the majority spin channel and 10 meV in the minority spin channel, leaving approximately 10 meV in each channel due to impurity scattering, probably from hydrogen as in the case of molybdenum discussed earlier.

It is interesting to note that when looking at unoccupied states the converse should be true.[62] At low temperatures, an electron added to an unoccupied minority spin band should decay preferentially via phonon scattering and an additional excited electron in a majority spin band should decay preferentially via magnon scattering.

Although non-spin resolved, another study has examined the possibility of scattering from spin excitations in the ferromagnetic material iron.[50] In studies of the Fe(001) surface Schafer *et al* identified a mass renormalization up to a binding energy of 120 meV. The latter energy was too large to be associated with phonons (Debye energy, $\theta_D \sim 39$ meV) and thus the authors identified the

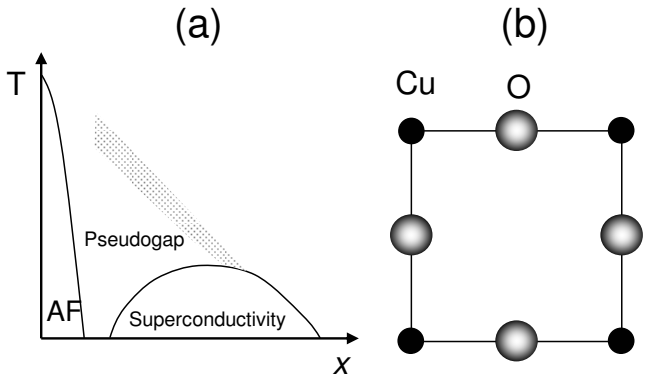

Figure 16: A schematic phase diagram showing the different ground states encountered in the cuprates as a function of temperature and doping. (b) The atomic layout of the copper oxygen planes that are thought to be responsible for the superconductivity in the cupartes.

self-energy corrections with scattering from spin excitations.

6 Studies of the High T_C Superconductors

In this final section we discuss studies of the high T_C superconductors and related compounds. As we have already noted, these materials discovered in 1986 [63] have presented and continue to present some of the biggest challenges in materials science today. ARPES with high energy and momentum resolution has emerged as one of the leading techniques for the study of such materials. Indeed it was the drive to understand the high T_C superconductors that led to a renaissance in the use of ARPES. The technique has made many important contributions to our understanding of these materials including measurements of the anisotropy of both the superconducting gap [64] [65] and the normal state "pseudogap". [66, 67] More recently, the discovery of a mass renormalization,[9] evident in the dispersion in the vicinity of the Fermi level of the cuprate, $Bi_2Sr_2CaCu_2O_{8+\delta}$, has led to renewed speculation about the origin of high temperature superconductivity and the possibility that the observed renormalization reflects coupling to some boson involved in the pairing.

Before discussing the renormalization effects in more detail we first review some aspects of the high T_C superconductors. It is generally accepted that the superconductivity in the cuprates evolves from a parent insulating state by doping carriers into the 2-dimensional CuO_2 planes. With half-filled band, the ground state of the parent compound is an antiferromagnetic Mott insulator. With doping, the systems move from the antiferromagnetic state through to a regime where superconductivity is possible. The commonly accepted phase diagram for the cuprates is shown in figure 16(a). The materials exhibit super-

conductivity in the region under the dome. However in the underdoped region a gap or "pseudogap" is observed in the normal state at temperatures well above the superconducting transition temperature, T_C. At optimal doping corresponding to the maximum T_C the materials are considered non-Fermi liquids in the normal state. The structure of the Cu-O plane is shown in figure 16(b). In the superconducting state the order parameter has d-wave symmetry. In terms of the Cu-O plane, the d-wave symmetry is reflected in the gap being maximum in the copper oxygen bond direction and non-existent in the direction along the diagonal or copper-copper direction. The latter corresponding to the (π, π) direction of the Brillouin zone is commonly referred to as the nodal direction and the former in the $(\pi, 0)$ direction of the Brillouin zone as the anti-nodal direction.

The first photoemission studies of the high T_C superconductors [68] [69] identified the copper d-bands and in the case of $YBa_2Cu_3O_{6+x}$, a Fermi level.[68] With improved crystals the superconducting gap was identified [70] followed by measurements of the anisotropy of the gap in the a-b plane associated with the d-wave symmetry.[64, 65] These studies were extended to similar measurements of the anisotropy of a pseudogap observed in the normal state in the underdoped materials.[66, 67] There have also been a number of studies of the spectral function in the vicinity of the $(\pi, 0)$ direction. In the superconducting state this is characterized by a "peak dip hump" structure similar to that in the vicinity of the gap in a BCS like superconductor. As such, the observation has promoted considerable discussion along the lines of the BCS mechanism. Reviews of much of this and previous work have been presented elsewhere.[71, 72]

In the present discussion we focus our attention on studies of the nodal region, primarily because a mass renormalization observed in spectra recorded in that direction has all the hallmarks of the mass renormalizations that we have discussed in earlier sections in this chapter. However, while we restrict our discussion to this region, observations in the nodal direction clearly have implications for observations throughout the zone.

The first high resolution study of the electronic structure in the nodal direction revealed a new feature, a mass enhancement of the low energy excitations immediately below the Fermi level.[9] The relevant spectral intensity plot has been shown earlier in figure 2. With certain assumptions about the non-interacting dispersion, the authors reported an increased effective mass m^* such that $m^*/m_b \sim 1.6$ where m_b represents the observed mass at higher binding energies. This observation has potentially important implications for the mechanism driving high T_C superconductivity and an obvious question is whether or not it points to a BCS like mechanism whereby the electrons or renormalization and associated "kink" have become central issues in subsequent ARPES work with considerable controversy regarding their source.[73, 74, 75, 76, 77] Are they related to the presence of spin excitations or do they reflect an interaction with phonons or indeed any other collective mode? In the case of the cuprates, this is not an easy issue to resolve as the various energy scales are nearly identical. However, there is broad agreement on the experimental observations.

All studies agree that the "coupling" is largest in the underdoped regime

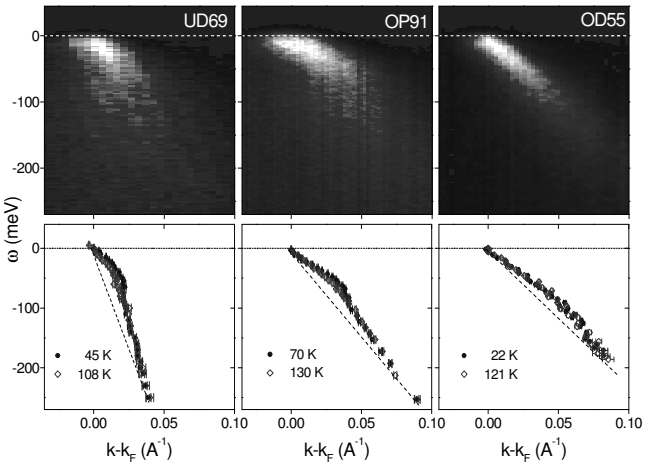

Figure 17: Upper panels: two dimensional photoemission intensities observed from (a) underdoped (UD), (b) optimally doped (OP), and (c) overdoped (OD) samples. The superconducting transition temperatures are indicated. Lower panels: the dotted lines indicate the MDC deduced dispersions for both the superconducting (blue dots) and normal states (open red diamonds) corresponding to the different samples in the panels above.

as is evident in the spectra of figure 17.[76] By coupling we mean, as discussed above, that the measured velocity is decreased compared to the bare velocity in the absence of coupling. However it has also been noted that the measured Fermi velocity shows little variation as a function of doping.[76] [78] Thus the biggest change is not in the measured velocity, rather it is in the assumed bare velocity, i.e. the "bare" velocity is largest in the underdoped regime. This is counterintuitive in that the underdoped regime is more insulating like and one would naively anticipate that the velocity would be less. Experimentally the observation of constant Fermi velocity is evident in spectra obtained from both the $Bi_2Sr_2CaCu_2O_{8+\delta}$ [76] and $L_{2-x}Sr_xCuO_4$ [78] families. It is also reproduced in certain theoretical calculations.[79]

In examining the mass enhancement some groups have focused more closely on the associated "kink" in the dispersion and suggested that its presence at a similar energy in studies of all of the different cuprates is an indication of coupling to a phonon mode.[75] Indeed neutron studies do indicate the presence of phonon modes at similar energies.[80] The authors of these studies have also suggested that an "unconventional isotope effect" is an indication of the role of phonons in that the substitution of O^{18} for O^{16} results in a change in the velocity of the higher energy electrons as opposed to the lower energy electrons in the vicinity of the Fermi level.[81] If the phonons play any role in the superconductivity, this observation is again counterintuitive. However we note that subsequent attempts to reproduce this effect have failed.[82] More recently,

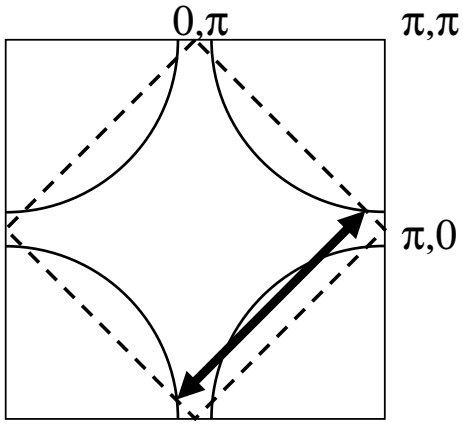

Figure 18: Fermi surface of a doped cuprate system (solid arcs) and the antiferromagnetic Brillouin zone of an undoped insulator (dashed line). Regions on the Fermi surface ("Hot spots") that can be joined by the double ended arrow representing the antiferromagnetic wave-vector (π, π) can be strongly coupled to antiferromagnetic fluctuations .

proponents of the phonon scenario have used the maximum entropy method (MEM) to extract an Eliashberg function, α^2F.[83] The results of this study suggest a multimode structure for the phonon spectrum. While this is a distinct possibility we note that the analysis is also controversial at the present time.[84, 85]

There are several observations that argue against phonons as the source of kink. Firstly, we note that certainly in the optimally doped materials the resistivity is perfectly linear down to the superconducting transition temperature. A linear resistivity can be associated with phonon scattering. However, as was noted with respect to equation (6) earlier, this linearity extends down to approximately one third the Debye energy. In the case of $L_{2-x}Sr_xCuO_4$, T_C is approximately 40 K. Multiplying by a factor of three would correspond to a Debye energy of 10 meV, which is certainly too low to give the observed "kink" in the photoemission spectrum at 70 meV. As such, if phonons are involved, the mechanism is certainly not describable using the standard Eliashberg approach. Further, the measured scattering rates do not saturate at energies above the kink energy as would be expected on the basis of the Eliashberg equation if the kink reflected the Debye energy. Rather they show a continuous variation to higher binding energies suggesting that some form of electron-electron scattering plays an important role.

An alternative scenario would suggest that the mass enhancement reflects coupling to the spin excitations in the system. Such a coupling is expected to be strongest in the anti-nodal or (π,0) region reflecting the observation that the spin excitations are described primarily by the scattering vector $Q = (\pi, \pi)$,

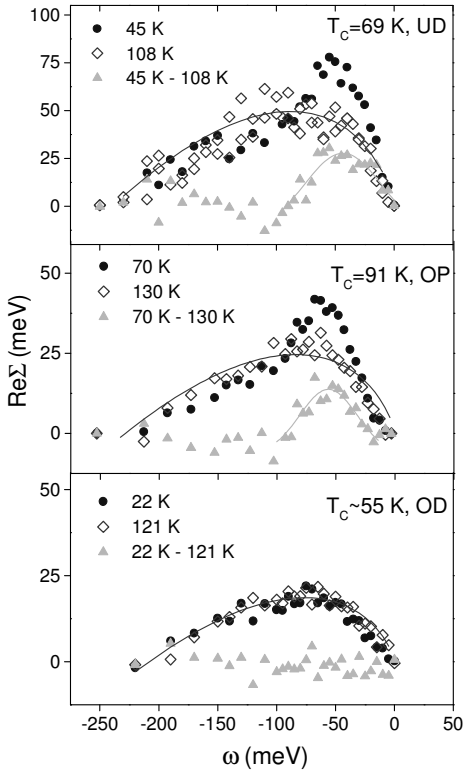

Figure 19: Σ_1 as a function of binding energy for the superconducting (blue dots) and normal states (open red diamonds) for the UD69, OP91, and OD55 samples. The solid lines through the normal state data represent MFL fits to the data. The difference between the superconducting and the normal Σ_1 for each level of doping is also plotted (green triangles). The lines through the latter are Gaussian fits to extract the peak energy ω_0^{sc}.

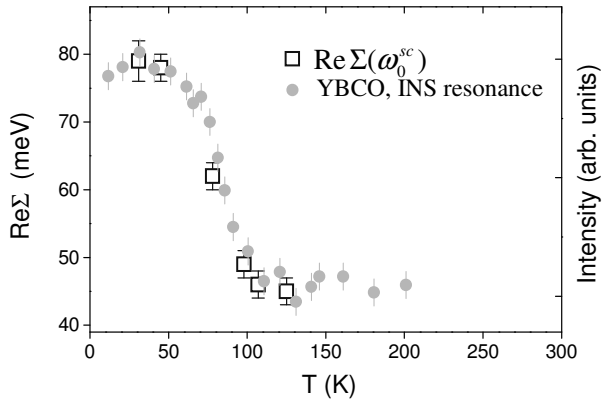

Figure 20: Temperature dependence of $\Sigma_1(\omega_0^{sc})$ from the nodal line for an underdoped sample with $T_c = 69$K (black squares) compared with the temperature dependence of the intensity of the resonance mode observed in INS studies of underdoped $YBa_2Cu_3O_{6+x}$, $T_C = 74$ K (Ref. [90]) (gray circles).

which couples the antinodal regions as shown if figure 18. However certain behavior in the nodal region would appear to carry the hallmarks of such an interaction. Examining figure 17 it is possible, with certain assumptions about the bare velocities, to extract representative doping dependent real components of the self energy, Σ_1. These are reproduced in figure 19 where for each doping level the Σ_1 corresponding to the superconducting state is compared to the Σ_1 corresponding to the normal state.[76] Certainly in the underdoped and optimally doped regimes there is a marked difference in the spectra on entering the superconducting state. Similar behavior has been observed elsewhere both in ARPES studies[12, 86] and in optical conductivity studies.[87] The changes in Σ_1 can be measured as a function of temperature as indicated in figure 20. From the latter figure we see a reasonably sharp onset around the superconducting transition temperature. Again similar data has been obtained in a more recent study reported by Terashima *et al.*[88] Many properties of the high T_C superconductors show a similar temperature dependence including the development of a sharp coherent peak in the $(\pi, 0)$ direction,[89] the development of the superconducting gap at the Fermi surface and the rearrangement of the spin susceptibility associated with the formation of a magnetic resonance mode in the superconducting state.[90] All of these changes are identified with the electron channel. As we have noted above, it is less clear that such a marked temperature dependence exists in the phonon spectrum. Several authors have therefore associated the changes observed in Σ_1 with changes observed in the spin susceptibility, pointing to scattering from spin excitations as the source of mass renormalization.[11, 76, 88, 91] This is consistent with the observation that the coupling appears much stronger in the underdoped regime, a region where the spin excitations are more pervasive. Further the effects become more

pronounced on moving away from the nodal direction towards the $(\pi, 0)$ direction. This is evident in the measured momentum dependence of the change in the Fermi velocity on entering the superconducting state[92] and is consistent with the observation that the spin excitations are described primarily by the scattering vector $Q = (\pi, \pi)$ coupling the antinodal regions.

7 Summary and outlook

The new experimental developments combined with new analysis methods have allowed photoemission to become a powerful probe of the collective excitations in condensed matter systems. We can anticipate that such studies will continue and be extended to an ever larger array of new materials. We can also anticipate that the experimental capabilities will be improved. However this will not be easy. The total energy resolution in any experiment is influenced by the energy spread in the incident light beam and the resolving power of the electron spectrometer. These each present a challenge but not an insurmountable challenge. The temperature of the sample and also the quality of the sample surface will also be reflected in the measured peak widths. These contributions are intrinsic and represent more of a challenge. It will be challenge to get the sample much below 1 K but getting to low temperatures is worth the effort. It is a simple matter to show from equation (6) above that in the limit of 0 K the Eliashberg function, $\alpha^2 F$, is simply related to $\frac{d\Delta k(\omega)}{d\omega}$ where $\Delta k(\omega)$ is the width of an MDC at binding energy ω. The problems associated with sample surface quality will be somewhat alleviated in experiments that are less surface sensitive such as the new laser based techniques.[93, 94]

Acknowledgments

We would like to acknowledge the many contributions of our collaborators on the work described here. These include A.V. Fedorov, S.L. Hulbert, P-A Glans, C. McGuinness, K.E. Smith. E.Y. Andrei, H. Berger, Q. Li, G.D. Gu, N. Koshizka, G. Reisfeld, J. Xue, F.J. DiSalvo, Z. Yusof, B.O. Wells, A.R. Moodenbaugh, C. Kendziora, S. Jian, D.G. Hinks, F. Liu, M. Weinert, T.E. Kidd and P.B. Allen. The research work described in this paper was supported by the Department of Energy under Contract No. DE-AC02-98CH10886.

References

[1] N. Martensson, P. Baltzer, P.A. Bruhweiler, J.-O. Forsell, A. Nilsson, A. Stenborg, and B. Wannberg, J. Electron Spectr. Relat. Phenom. , 70 117, (1994)

[2] J.G. Bednorz and K.A. Muller, Zeit. Phys. B, 64, 189 (1986)

[3] D. Pines and P. Nozieres, *The Theory of Quantum Liquids* (Benjamin, New York, 1969).

[4] N.V. Smith, P. Thiry, and Y. Petroff, Phys. Rev. B 47, 15476 (1993)

[5] G.D. Mahan, *Many Particle Physics*, Plenum Press, New York 1990.

[6] N. V. Smith *et al*, Phys. Rev. B 64, 155106 (2001).

[7] *Angle-Resolved Photoemission*, Ed. S. Kevan, Elsevier Amsterdam 1992.

[8] G. Grimvall, *The Electron-Phonon Interaction in Metals* (North- Holland, New York, 1981).

[9] T. Valla at al, Science 285, 2110 (1999);

[10] S. LaShell, E. Jensen and T. Balasubramanian, Phys. Rev. B 61, 2371 (2000)

[11] A. Kaminski *et al.*, Phys. Rev. Lett. 84, 1788 (2000)

[12] T. Valla *et al*, Phys. Rev. Lett. 85, 4759 (2000).

[13] A.A. Kordyuk *et al.*, Phys. Rev. B, 71, 214513 (2005)

[14] B.A. McDougall, T. Balasubramanian and E. Jensen, Phys. Rev. B 51, 13891 (1995)

[15] T. Balasubramanian, E. Jensen, X.L. Wu, and S.L. Hulbert, Phys. Rev B 57, R6866 (1998)

[16] M. Hengsberger *et al*, Phys. Rev. Lett. 83, 592 (1999).

[17] T. Valla, A. V. Fedorov, P. D. Johnson and S. L. Hulbert, Phys. Rev. Lett. 83, 2085 (1999)

[18] K. Jeong, R H. Gaylord and S. D. Kevan, Phys. Rev. B 38, 10302 (1988); K. Jeong, R H. Gaylord and S. D. Kevan, Phys. Rev. B 39, 2973 (1989).

[19] S. Y. Savrasov and D. Y. Savrasov, Phys. Rev. B 54, 16487 (1996).

[20] C. Hodges, H. Smith and J. W. Wilkins, Phys. Rev. B 4, 302 (1971).

[21] W. A. Harrison, Electronic Structure and the Properties of Solids (W. H. Freeman & Co, San Francisco, 1980).

[22] J. A. Wilson, F. J. Di Salvo and S. Mahajan, Phys. Rev. Lett. 32, 882 (1974).

[23] A. H. Castro Neto, Phys. Rev. Lett. 86, 4382 (2001).

[24] F. Smith *et al*, J. Phys. C: Solid State Phys. 5, L230 (1972); C. Berthier, P. Molini'e and D. J'erome, Solid State Commun. 18, 1393 (1976); D. W. Murphy *et al*, J. Chem. Phys. 62, 967 (1975).

[25] P. Moline, D. Jerome and A. J. Grant, Phil. Mag. 30, 1091 (1974).

[26] H. Suderow, V.G. Tissen, J.P. Brisson, J.L. Martinez, and S. Vieira, Phys. Rev. Lett., 95, 117006 (2005)

[27] P. Garoche *et al*, Solid State Commun. 19, 455 (1976); D. Sanchez *et al*, Physica B 204, 167 (1995).

[28] J. E. Graebner and M. Robbins, Phys. Rev. Lett. 36, 422 (1976).

[29] R. Corcoran *et al*, J. Phys.: Condens.Matter 6, 4479 (1994).

[30] T. Yokoya *et al*, Science 294, 2518 (2001); T. Kiss *et al*, Physica B 312-313, 666 (2002).

[31] J. A. Wilson, Phys. Rev. B 15, 5748 (1977).

[32] N. J. Doran *et al*, J. Phys. C 11, 699 (1978).

[33] T. M. Rice and G. K. Scott, Phys. Rev. Lett. 35, 120 (1975).

[34] B. Ruzicka at al, Phys. Rev. Lett. 86, 4136 (2001).

[35] K. Rossnagel, E. Rotenberg, H. Koh, N.V. Smith and L. Kipp, Phys. Rev. B, 72, 121103 (2005)

[36] R. Liu, C.G. Olson, W.C. Tonjes, and R.F. Frindt, Phys. Rev. Lett. 80, 5762 (1998)

[37] R. Liu *et al*, Phys. Rev. B 61, 5212 (2000).

[38] Th. Straub *et al*, Phys. Rev. Lett. 82, 4504 (1999).

[39] G. Benedek *et al*, Europhys. Lett. 5, 253 (1988); G. Brusdeylins *et al*, Phys. Rev. B 41, 5707 (1990).

[40] T. Valla, A.V. Fedorov, P.D. Johnson, P-A Glans, C. McGuinness, K.E. Smith. E.Y. Andrei and H. Berger, Phys. Rev. Lett. 92, 086401 (2004)

[41] J. L. Feldman, Phys. Rev. B 25, 7132 (1982); G. Brusdeylins *et al*, Phys. Rev. B 41, 5707 (1990); Y. Nishio, J. Phys. Soc. Jpn. 63, 223 (1994).

[42] J. M. E. Harper, T. H. Geballe and F. J. DiSalvo, Phys. Rev. B 15, 2943 (1977); K. Noto, N. Kobayashi and Y. Muto, Nuovo Cimento 38, 511 (1977).

[43] S. V. Dordevic, D. N. Basov, R. C. Dynes and E. Bucher, Phys. Rev. B 64, 161103 (2001).

[44] R. Liu *et al*, Phys. Rev. B 61, 5212 (2000); A. V. Fedorov *et al*, unpublished.

[45] Th. Straub *et al*, Phys. Rev. Lett. 82, 4504 (1999).

[46] W. C. Tonjes *et al*, Phys. Rev. B 63, 235101 (2001).

[47] H. F. Hess *et al*, J. Vac. Sci. Technol. A 8, 450 (1990).

[48] A.V. Fedorov, T. Valla, D.J. Huang, G. Reisfeld, F. Loeb, F. Liu and P.D. Johnson, J. Elect. Spectr. And Relat. Phenom. 92, 19 1998.

[49] A.V. Fedorov, T. Valla, F. Liu, P.D. Johnson, M. Weinert and P.B. Allen, Phys. Rev. B 65, 212409 (2002)

[50] J. Schafer, D. Schrupp, E. Rotenberg, K. Rossnagel, H. Koh, P. Blaha and R. Claessen, Phys. Rev. Lett. 92, 97205 (2004)

[51] P.D. Johnson. Rep. Prog. Phys. 60, 1217-1304 (1997)

[52] R. Wu, C. Li, A.J. Freeman and C.L. Fu, Phys. Rev. B 44, 9400 (1991).

[53] D. Li, C.W. Hutchings, P.A. Dowben, C. Hwang, R.T. Wu, M. Oneelion, A.B. Andrews, J.L. Erskine, J. Magn. Magn. Mater. 99, 85 (1991)

[54] G.A. Mulhollan, K. Garrison and J.L. Erskine, Phys. Rev. Lett. 69, 3240 (1992)

[55] P. Wells, P.C. Lanchester, P.W. Jones and R.G. Jordan, J. Phys. F, 4, 1729 (1974)

[56] H.L. Skriver and I. Mertig, Phys. Rev. B 41, 6553 (1990)

[57] D. Li, J. Zhang, P.A. Dowben, K. Garrison, P.D. Johnson, H. Tang, T. G. Walker, H. Hopster, J.C. Scott, D. Weller and D.P. Pappas, Mat. Res. Socs Proc. 313, 451 (1993)

[58] A.V. Fedorov, K. Starke and G. Kaindl, Phys. Rev. B 50, 2739 (1994); E. Weschke, C. Schussler- Langeheine, R. Meier, A.V. Fedorov, K. Starke, F. Hubinger and G. Kaindl, Phys. Rev. Lett. 77, 3415 (1996).

[59] B. Sinkovic, E. Shekel and S.L. Hulbert, Phys. Rev. B, 52, R15703 (1995).

[60] P.B. Allen, Phys. Rev. B 63, 214410 (2001)

[61] C. Zener, Phys. Rev. 81, 440 (1951); C. Zener, Phys. Rev. 82, 403 (1951); C. Zener, Phys. Rev. 83, 299 (1951).

[62] A. Rehbein, D. Wegner, G. Kaindl, and A. Bauer, Phys. Rev. B 67, 033403 (2003)

[63] J.G. Bednorz and K.A. Muller, Z. Phys. B: Condens. Matter, 64, 189 (1986)

[64] Z.X. Shen, D.S. Dessau, B.O. Wells *et al.*, Phys. Rev. Lett. 70, 1553 (1993)

[65] H. Ding *et al.*, Phys Rev Lett., 74, 2784 (1995)

[66] A.G. Loeser *et al.*, Science 273, 325 (1996)

[67] H. Ding *et al.*, Nature 382, 51 (1996)

[68] B. Reihl, T. Riesterer, J.G. Bednorz and K.A. Muller, Phys. Rev. B 35, 8804 (1987)

[69] P.D. Johnson, S.L. Qiu, L. Jiang, M.W. Ruckman, M. Strongin, S.L. Hulbert, R.F. Garrett, B. Sinkovic, N.V. Smith, R.J. Cava, C.S. Jee, D. Nichols, Kaczanowicz, R.E. Salomon, and J.E. Crow, Phys. Rev. B 35, 8811 (1987).

[70] C.G. Olsen *et al.*, Science245, 731 (1989)

[71] A. Damascelli, Z. Hussain, and Z.-X. Shen, Rev. Mod. Phys. 75, 473 (2003)

[72] J.C. Campuzano, M.R. Norman and M Randeiria in *Physics of Superconductors ,* Vol.II, ed K.H. Bennemann and J.B. Ketterson, Springer Berlin, 2004 p. 167-272

[73] P. V. Bogdanov at al, Phys. Rev. Lett. 85, 2581 (2000)

[74] A. Kaminski *et al*, Phys. Rev. Lett. 86, 1070 (2001).

[75] A. Lanzara *et al*, Nature 412, 510 (2001).

[76] P. D. Johnson *et al*, Phys. Rev. Lett. 87, 177007 (2001).

[77] T. K. Kim *et al*, Phys. Rev. Lett. 91, 167002 (2003).

[78] X.J. Zhou *et al.*, Nature 423, 398 (2003)

[79] M. Randeria, A. Paramekanti and N. Trivedi, Phys. Rev. B 69 144509 (2004)

[80] R.J. McQueeney *et al.*, Phys. Rev. lett. 82, 628 (1999)

[81] G.-H. Gweon *et al.*, Nature, 430, 187 (2004)

[82] F. Douglas *et al.*, to be published

[83] X.J. Zhou, Phys. Rev. Lett., 95, 117001 (2005)

[84] T. Valla, cond-mat/0501138 (2005)

[85] X.J. Zhou *et al.* cond-mat/0502040 (2005)

[86] T. Yamasaki *et al.*, cond-mat/0603006 (2006)

[87] J. Hwang, T. Timusk and G.D. Gu, Nature, 427, 714, (2004)

[88] K. Terashima, H. Matsui, D. Hashimoto, T. Sato, T. Takahash, H. Ding, T. Yamamoto and K. Kadowaki, Nature Physics, 2, 27 (2006)

[89] A.V. Fedorov, T. Valla, P.D. Johnson, Q. Li, G.D. Gu and N. Koshizuka, Phys. Rev. Lett., 82, 2179 (1999)

[90] P. Dai *et al*, Science 284, 1346 (1999)

[91] T. Valla, Proceedings SPIE – Volume 5932, *Strongly Correlated Electron Materials: Physics and Nanoengineering*, Ivan Bozovic, Davor Pavuna Editors, 593203 (2005)

[92] T. Valla *et al*, Phys. Rev. Lett. 85, 828 (2000).

[93] T. Kiss *et al.*, Phys Rev. Lett., 94, 057001(2005)

[94] J.D. Koralek *et al.*, Phys. Rev. Lett. 96, 017005 (2006)